

Supporting Information

Hydroxymethyl Functionalized PEDOT-MeOH:PSS for Perovskite Solar Cells

*Hao Dong, Erjin Zheng, Zhiyin Niu, Xiaoyu Zhang, Yi-Yu Lin, Priyesh Jain, and Qiuming Yu**

Department of Chemical Engineering, University of Washington, Seattle, Washington 98195,
United States

E-mail: qyu@uw.edu

PEDOT-MeOH Synthesis and Possible Polymerization Mechanism

Table S1. The molar ratios of PSSH, Na₂SO₈, Fe₂(SO₄)₃, and NaOH to monomer EDOT-MeOH used for the synthesis of PEDOT-MeOH:PSS. Samples are presented by the amount of PSSH and Fe₂(SO₄)₃ used in the synthesis. PSS100 denotes the molar ratio of the repeated units of PSSH to those of PEDOT-MeOH 4.64:1, n/n, which is the same as PSS to PEDOT for the commercial AI 4083. PSS80 and PSS60 represent the amount of PSSH as 80% and 60% of the original amount of PSSH used in the synthesis, respectively. The L and H denote the low and high amount of Fe₂(SO₄)₃ used in the synthesis, respectively.

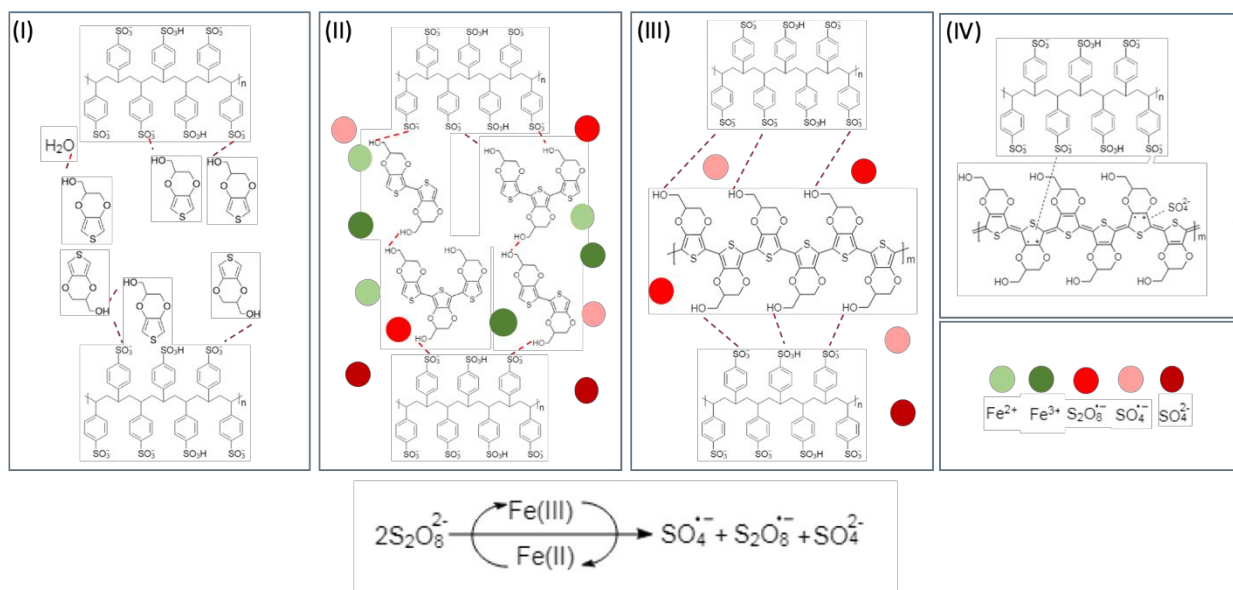
Sample	PSSH/ EDOT-MeOH	Na ₂ S ₂ O ₈ / EDOT-MeOH	Fe ₂ (SO ₄) ₃ / EDOT-MeOH	NaOH/ EDOT-MeOH
PSS100-L	4.64	4.47	0.05	2.32
PSS100-H	4.64	4.47	0.63	2.32
PSS80-L	3.71	4.47	0.05	1.86
PSS80-H	3.71	4.47	0.63	1.86
PSS60-L	2.78	4.47	0.05	1.39
PSS60-H	2.78	4.47	0.63	1.39

During the course of polymerization, the mixtures went through the distinct changes. An emulsion was formed when mixed PSSH and EDOT-MeOH monomer in DI water because PSSH has both hydrophobic backbone and hydrophilic sulfonic acid side groups but EDOT-MeOH is hydrophobic. EDOT-MeOH monomers either diffused into the hydrophobic core of PSSH or formed hydrogen bonding with sulfonic acid in water. The emulsion of EDOT-MeOH and PSSH turned blue from yellow within 10 min after Na₂S₂O₈ and Fe₂(SO₄)₃ solution and the half volume of NaOH were added. By then, the remaining half volume of NaOH solution was slowly added

into the emulsion in 3 h using a syringe pump. After stirring for 1-2 h since the beginning of reaction, the emulsion turned to darker blue and became more viscous to the point that stirring was difficult and some big particles were formed. More particles were observed for the batches with the high molar ratio of $\text{Fe}_2(\text{SO}_4)_3/\text{EDOT-MeOH}$. After stirring for 5-6 h, the particles gradually disappeared, and the mixture turned to less viscous. Finally, after 24 h, the dark blue emulsion was obtained with no precipitates.

Based on the experimental observations and previous studies of the oxidative chemical polymerization of PEDOT:PSS,¹⁻³ we proposed a possible polymerization mechanism for PEDOT-MeOH as shown in Scheme S1. EDOT-MeOH monomers can form hydrogen bonds with PSS and water as well as among monomers (Scheme S1I). Similar to the previous studies for PEDOT:PSS,⁴⁻⁶ ferric sulfate ($\text{Fe}_2(\text{SO}_4)_3$) oxidized EDOT-MeOH monomer into a cation radical that dimerized and was stabilized by the removal of two protons. Dimers were further oxidized by Fe^{3+} ions to form cation radicals, and short-chain polymers formed as a classical stepwise polymerization (Scheme S1II). The high oxidizability of ferric sulfate caused the polymerization to proceed quickly, thereby generating more short-chain polymers, or EDOT-MeOH oligomers. Hydrogen bonding between EDOT-MeOH oligomer and PSS as well as among EDOT-MeOH oligomers caused the mixture viscosity increasing. In the meantime, EDOT-MeOH oligomers formed insoluble particles in water phase. Adding one order of magnitude higher $\text{Fe}_2(\text{SO}_4)_3$ to the reaction mixture greatly accelerated the initial oxidization of monomers, forming a relatively large number of EDOT-MeOH oligomers, therefore, more insoluble particles in water. Adding sodium persulfate together with ferric sulfate in the initial period allowed slow polymerization and promoted the growth of longer polymer chain.⁴ The $\text{Fe}^{3+}/\text{Fe}^{2+}$ couples catalyzed the decomposition of persulfate ions $\text{S}_2\text{O}_8^{2-}$ into persulfate radical ($\text{S}_2\text{O}_8^{\cdot-}$) and sulfate radical ($\text{SO}_4^{\cdot-}$) (Scheme S1),

which oxidized EDOT-MeOH oligomers to form long-chain PEDOT-MeOH polymers (Scheme S1III). The oxidized PEDOT-MeOH backbones that were then doped by the negatively charged PSS (Scheme S1IV). Adding NaOH in the initial period adjusted the pH value of the reaction mixture, reducing the reactivity of $\text{Fe}^{3+}/\text{Fe}^{2+}$.⁷ Slowly adding the rest half volume of NaOH in the first 3 h made polymerization in a controllable way and deprotonated PSSH to better dope oxidized PEDOT-MeOH backbone. The hydrogen bonding dominated interaction between PEDOT-MeOH and PSS turned into a more electrostatic interaction, and a PEDOT-MeOH core-PSS shell structure was formed, which greatly reduced the viscosity of the mixture. The large EDOT-MeOH oligomer particles in water were gradually polymerized, oxidized and formed the core-shell structure. By the end of reaction, the mixture became a dark blue soluble emulsion.



Scheme S1. Schematic description of the possible stages in the oxidative chemical polymerization of PEDOT-MeOH:PSS.

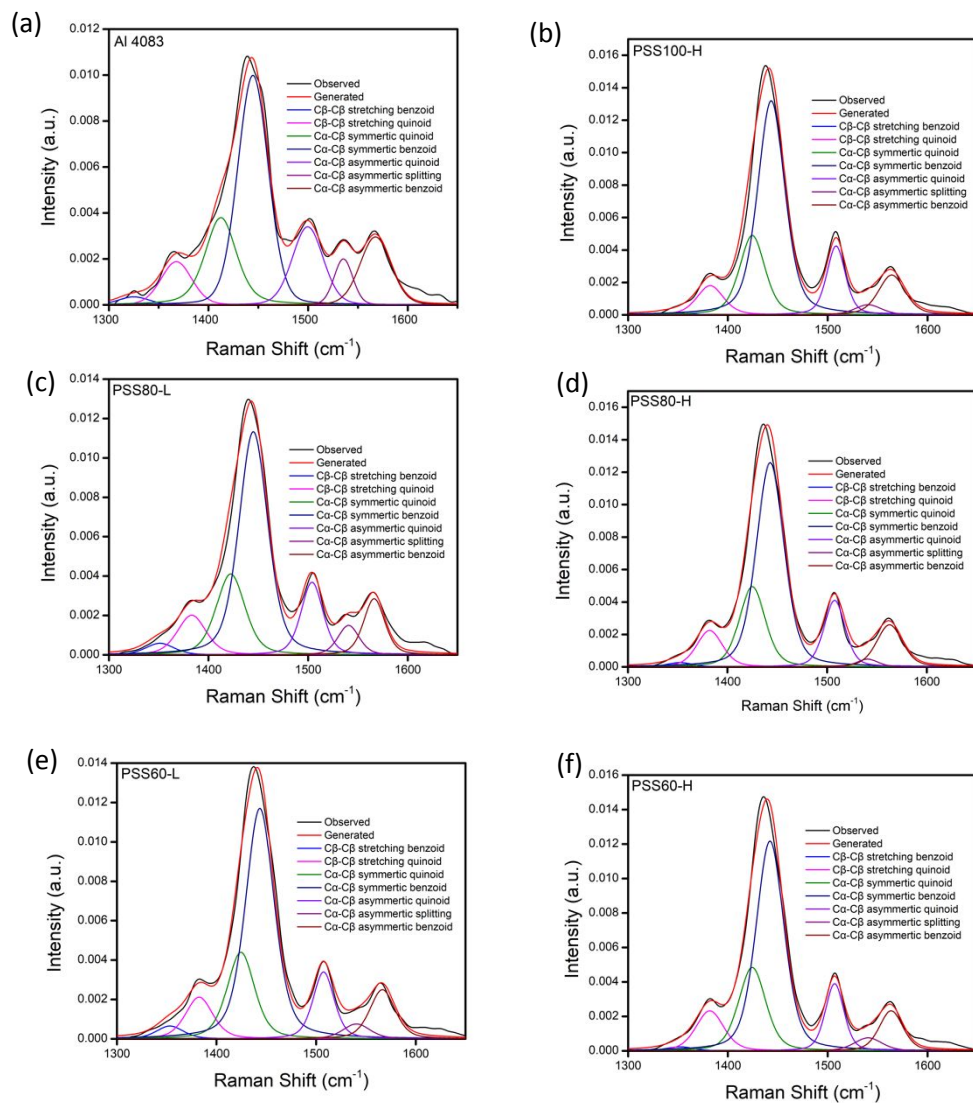


Figure S1. Deconvoluted Raman spectra of pristine thin films of (a) AI 4083 PEDOT:PSS, (b) PSS100-H, (c) PSS80-L, (d) PSS80-H, (e) PSS60-L, and (f) PSS60-H.

Table S2. Raman peak positions of the commercial AI 4083 PEDOT:PSS and PEDOT-MeOH:PSS with or without EG.

HTL	EG Content (vol%)	C _β -C _β stretching benzoid	C _β -C _β stretching quinoid	C _α -C _β symmetric stretching quinoid	C _α -C _β symmetric stretching benzoid	C _α -C _β asymmetric stretching quinoid	C _α -C _β asymmetric splitting	C _α -C _β asymmetric stretching benzoid
AI 4083	\	1332	1371	1417	1445	1499	1537	1570
PSS100-L	\	1351	1383	1421	1445	1502	1541	1568
PSS100-H	\	1351	1383	1421	1445	1502	1541	1568
	2	1353	1383	1424	1444	1508	1541	1567
	3	1351	1382	1424	1442	1508	1548	1564
	5	1351	1385	1429	1449	1505	1539	1567
PSS80-L	\	1352	1386	1428	1449	1504	1539	1565
PSS80-H	\	1354	1384	1426	1446	1505	1539	1566
	2	1352	1382	1424	1444	1508	1549	1564
	3	1352	1382	1424	1444	1508	1549	1564
	5	1352	1382	1424	1444	1508	1549	1564
	6	1355	1385	1427	1447	1508	1549	1564
PSS60-L	\	1355	1385	1426	1446	1508	1549	1564
PSS60-H	\	1352	1382	1424	1444	1508	1549	1564
	2	1352	1382	1424	1444	1508	1549	1564
	3	1355	1385	1427	1447	1507	1549	1564
	5	1355	1385	1427	1447	1508	1549	1564

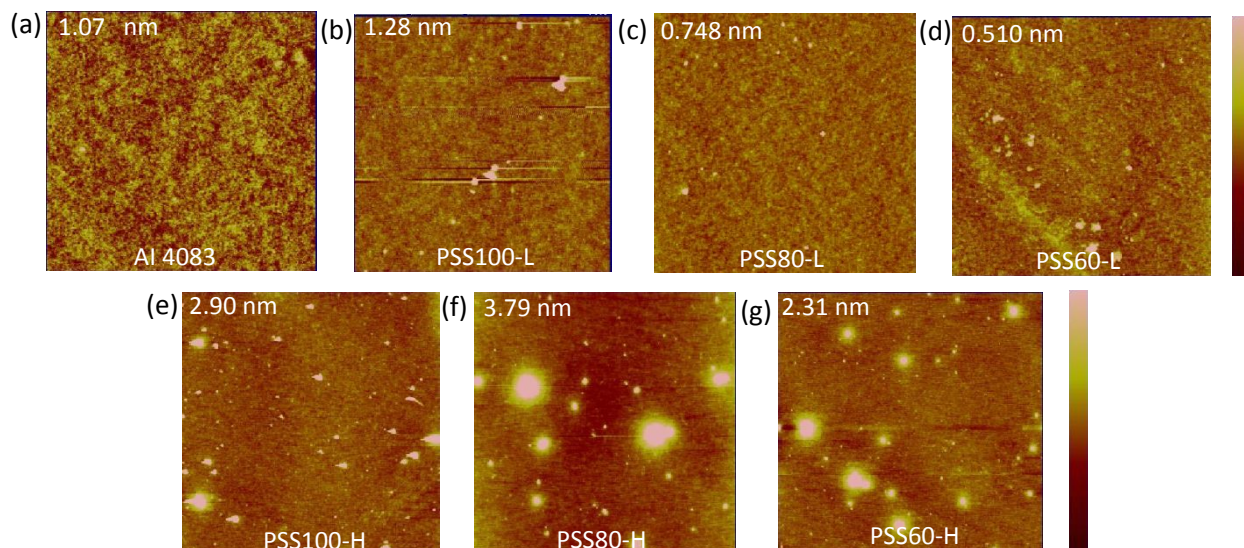


Figure S2. Large area ($10 \times 10 \mu\text{m}^2$) topographic AFM images of pristine thin films of (a) AI 4083 PEODT:PSS, (b) PSS100-L, (c) PSS80-L, (d) PSS60-L, (e) PSS100-H, (f) PSS80-H, and (g) PSS60-H. The Z scale is 10 nm. The root mean square (RMS) roughness of each surface is shown in the corresponding image.

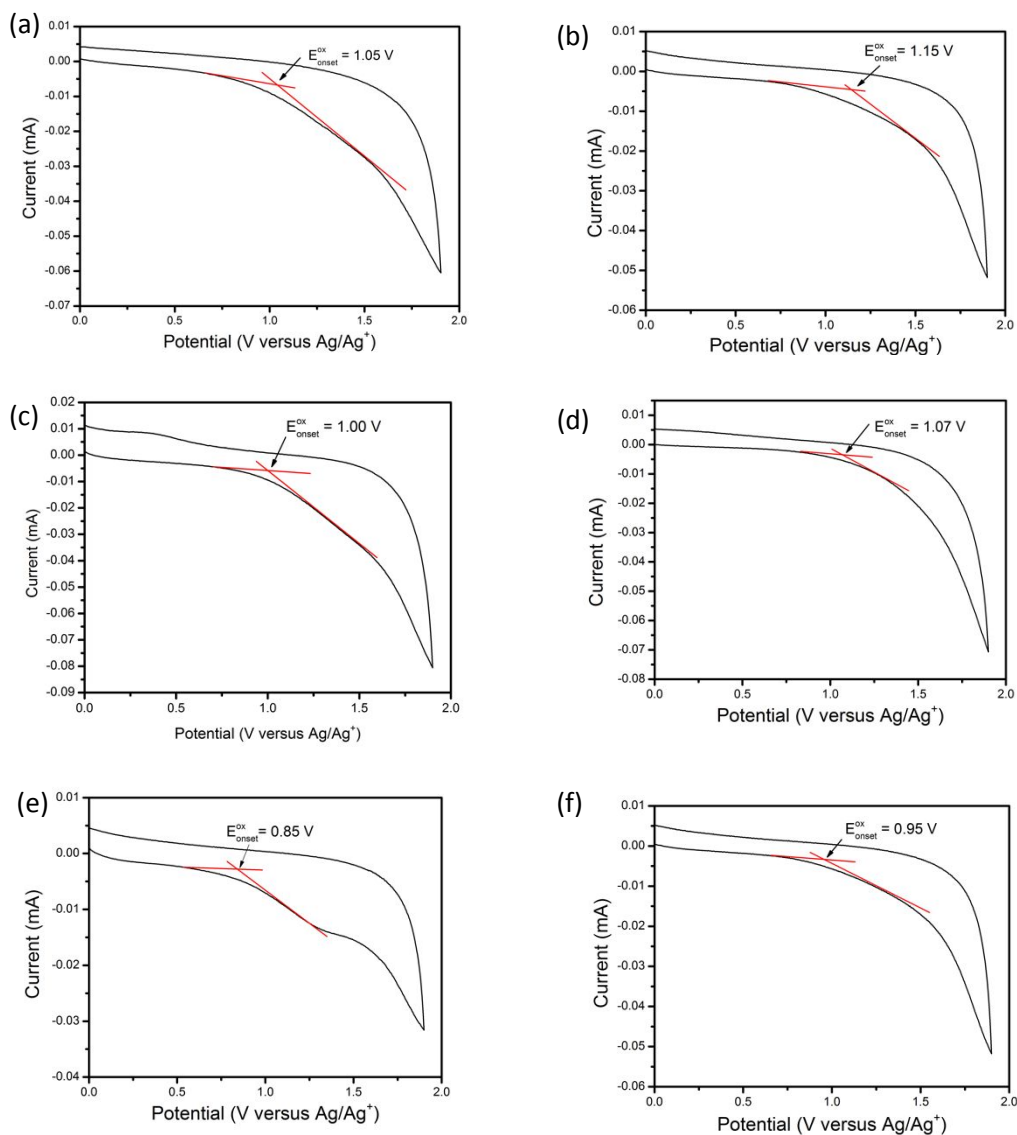


Figure S3. Cyclic voltammograms of (a) PSS100-L, (b) PSS100-H, (c) PSS80-L, (d) PSS80-H, (e) PSS60-L and (f) PSS60-H. During the experiment, the potential values were obtained in reference to the Ag/Ag^+ electrode and were then converted in reference to the internal standard of ferrocenium/ferrocene (Fc^+/Fc). Next, the potential values referenced to the Fc^+/Fc redox couple were converted to reference a saturated calomel electrode (SCE) and used along with empirical correlations to estimate the work function of PEDOT-MeOH:PSS samples.

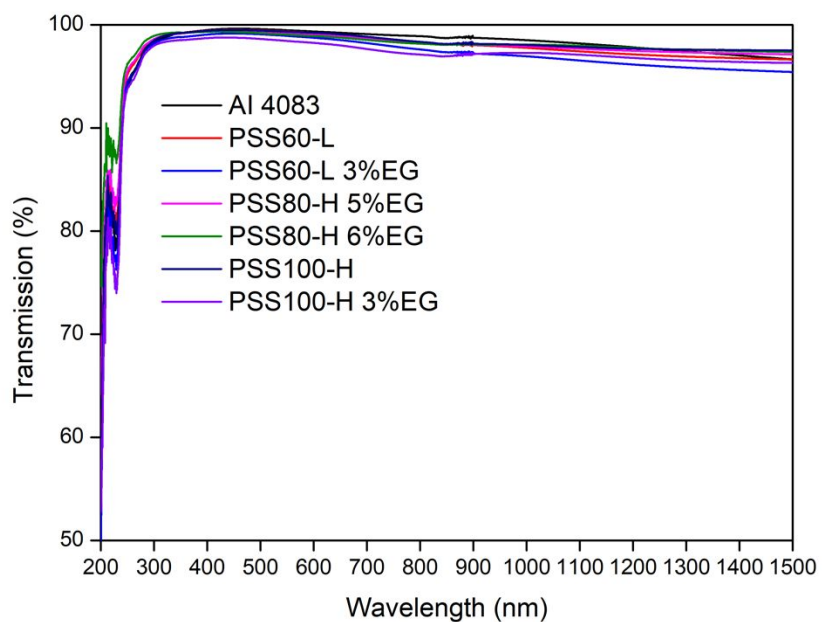


Figure S4. UV-Vis transmission spectra of AI 4083, PSS60-L, PSS60-L with 3% EG, PSS80-H with 5% EG, PSS80-H with 6% EG, PSS100-H, and PSS100-H with 3% EG.

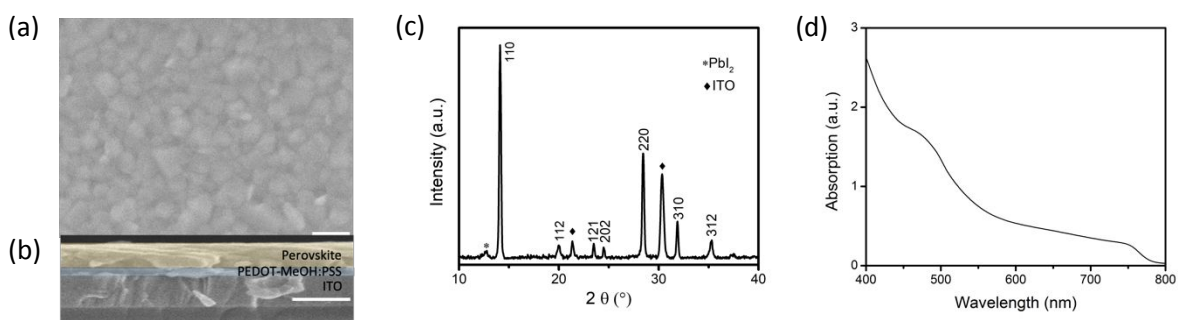


Figure S5. (a) Top and (b) cross-section SEM images and (c) XRD pattern of MAPbI_3 perovskite thin film fabricated on PSS80-H PEDOT-MeOH:PSS thin film on ITO/glass substrates. The scale bars are 200 nm. The peaks located at 21.5° and 30.3° are attributed to ITO. (d) UV-Vis absorption spectrum of MAPbI_3 perovskite thin film fabricated on PSS80-H PEDOT-MeOH:PSS thin film on glass substrate.

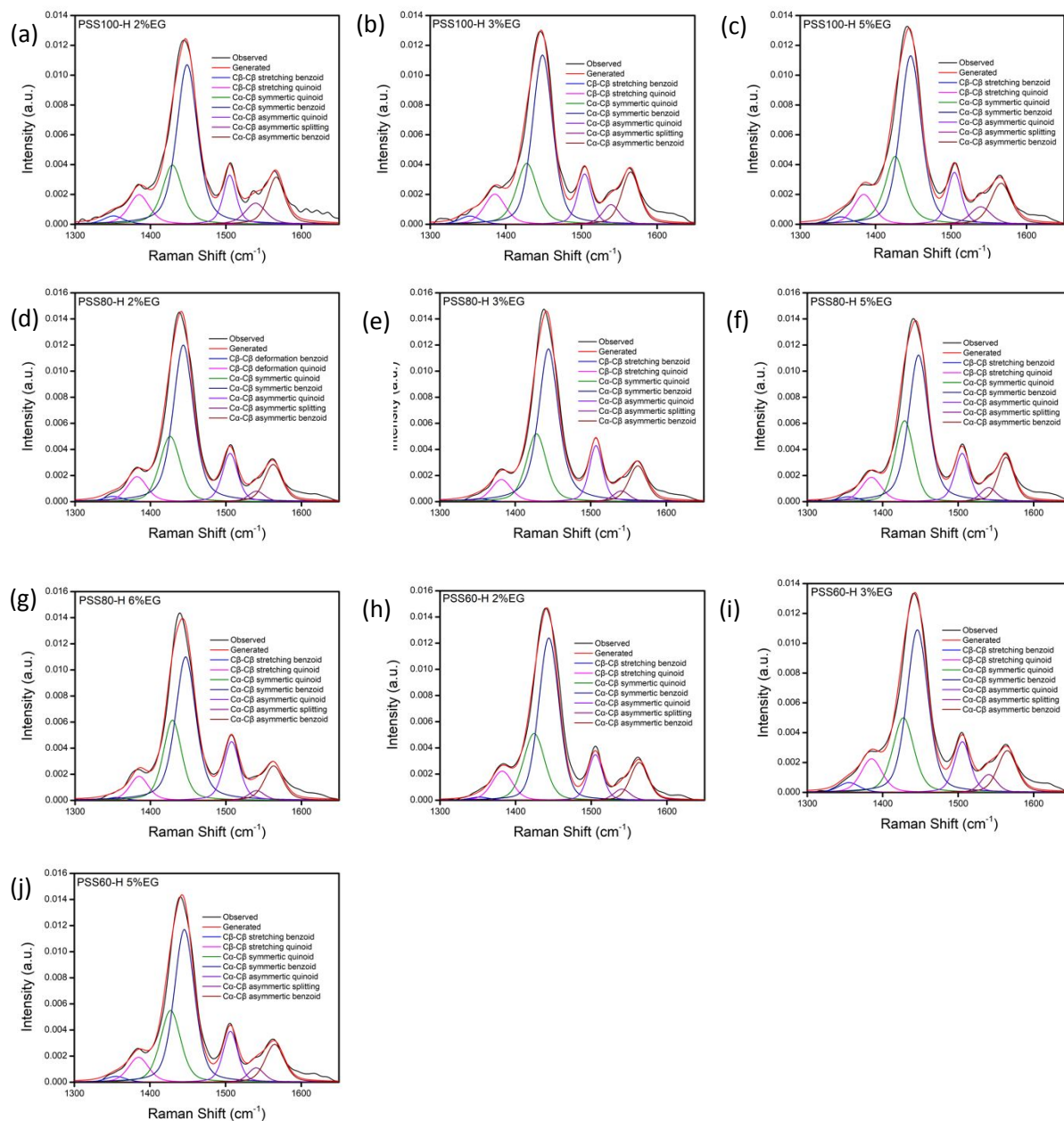


Figure S6. Deconvolution of Raman spectra of the thin films of PSS100-H with (a) 2 vol% EG, (b) 3 vol% EG, and (c) 5 vol% EG, PSS80-H with (d) 2 vol% EG, (e) 3 vol% EG, (f) 5 vol% EG, and (g) 6 vol% EG, and PSS60-H with (h) 2 vol% EG, (i) 3 vol% EG, and (j) 5 vol% EG.

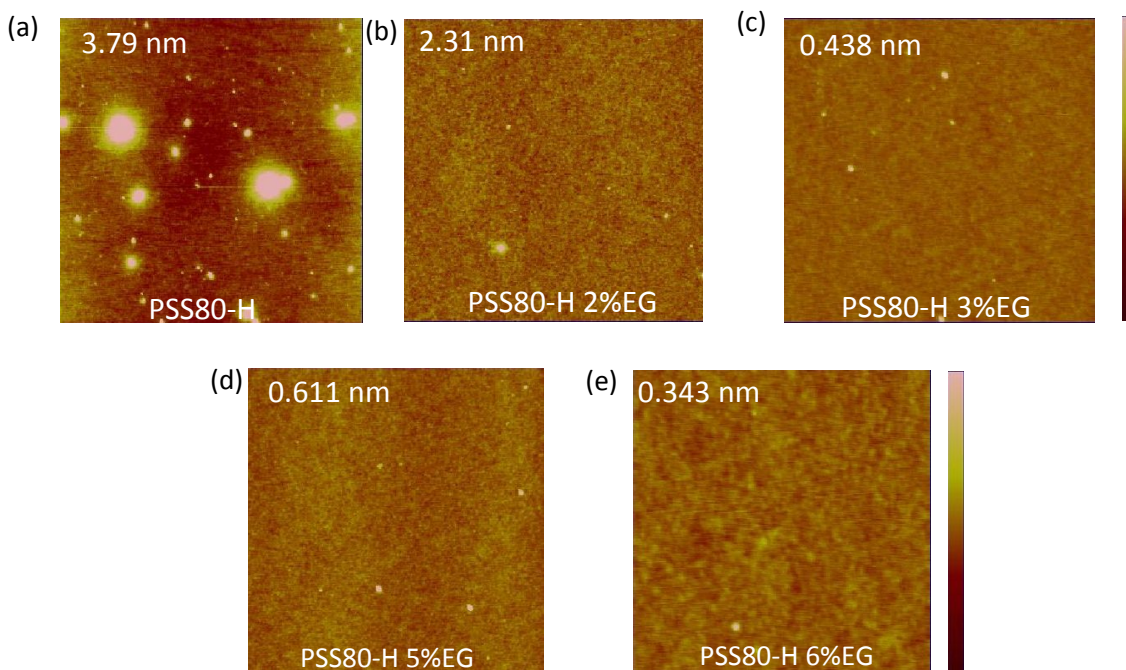


Figure S7. Large-scale (10 × 10 μm²) topographic AFM images of PSS80-H with (a) 0 vol% EG, (b) 2 vol% EG, (c) 3 vol% EG, (d) 5 vol% EG, and (e) 6 vol% EG. The Z scale is 10 nm. The RMS roughness of the surface is shown on the top left corner of the corresponding image.

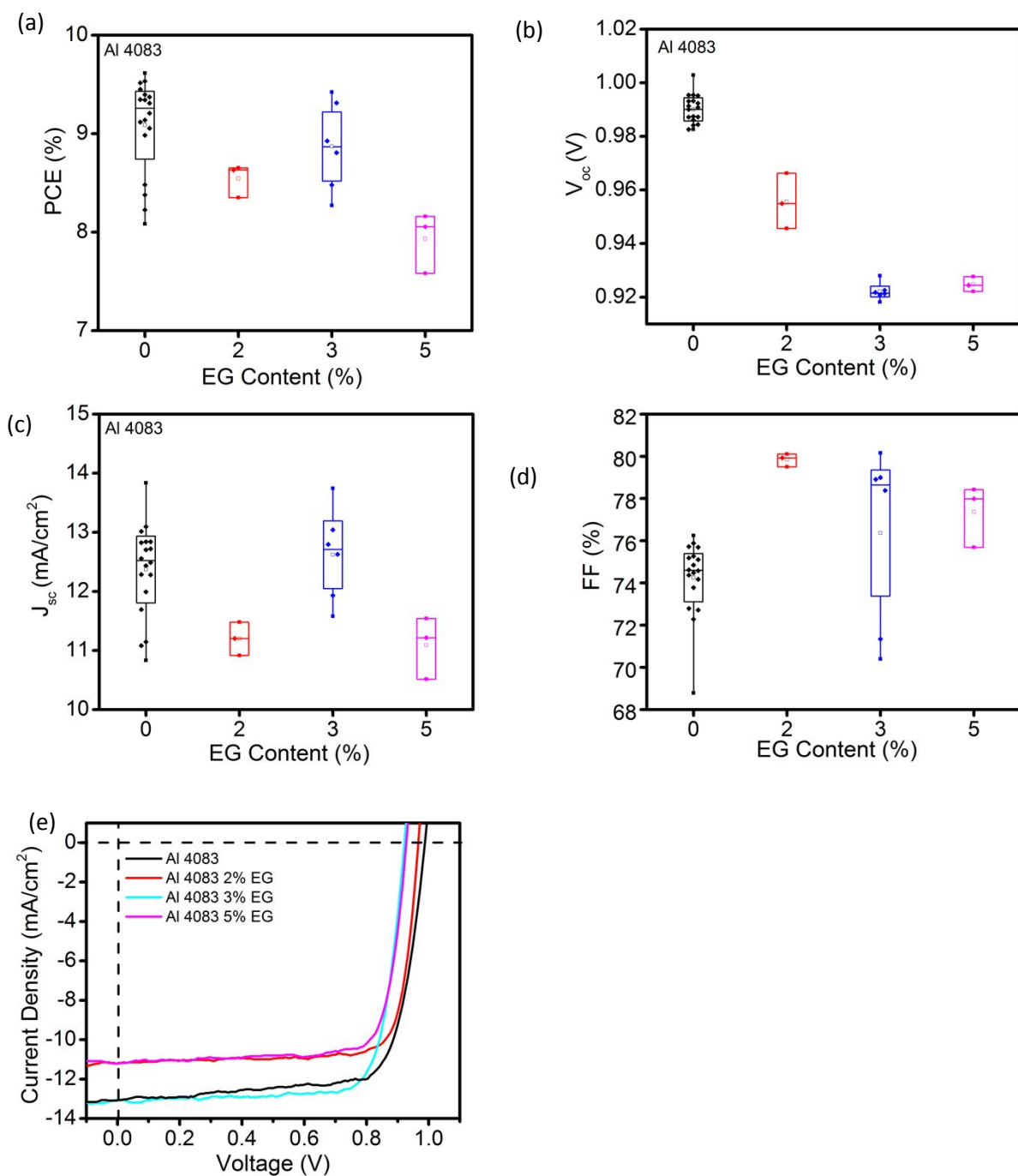


Figure S8. Statistics of (a) PCE, (b) V_{oc} , (c) J_{sc} , and (d) FF of the MAPbI₃ PVSCs based on AI 4083 PEDOT:PSS with and without EG. (e) $J-V$ curves of the best performance MAPbI₃ PVSCs based on pristine and 2, 3 and 5 vol% EG treated AI 4083 PEDOT:PSS HTLs.

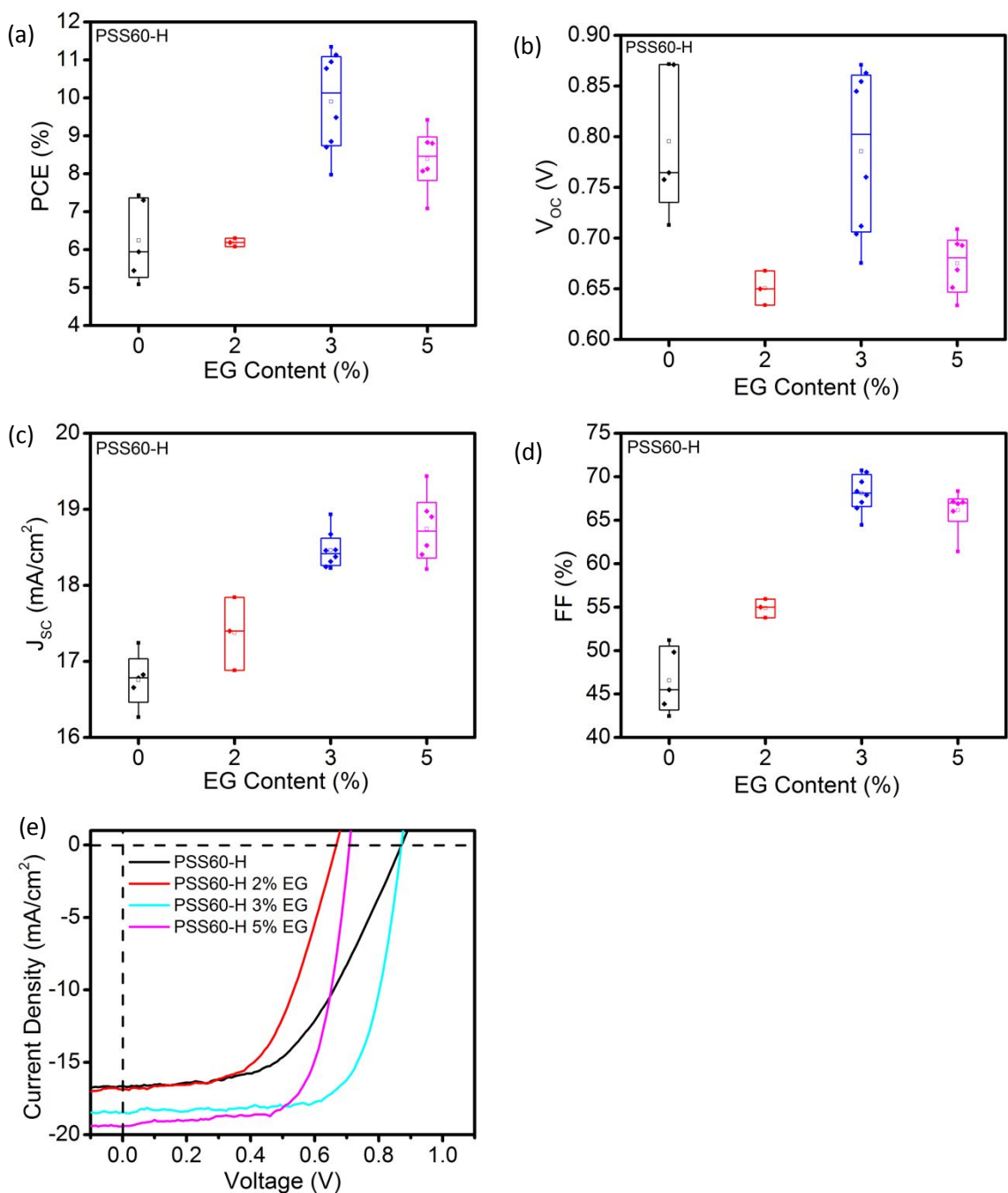


Figure S9. Statistics of (a) PCE, (b) V_{oc} , (c) J_{sc} , and (d) FF of the MAPbI₃ PVSCs based on PSS60-H with and without EG. (e) $J-V$ curves of the best performance MAPbI₃ PVSCs based on pristine and 2, 3 and 5 vol% EG treated PSS60-H HTLs.

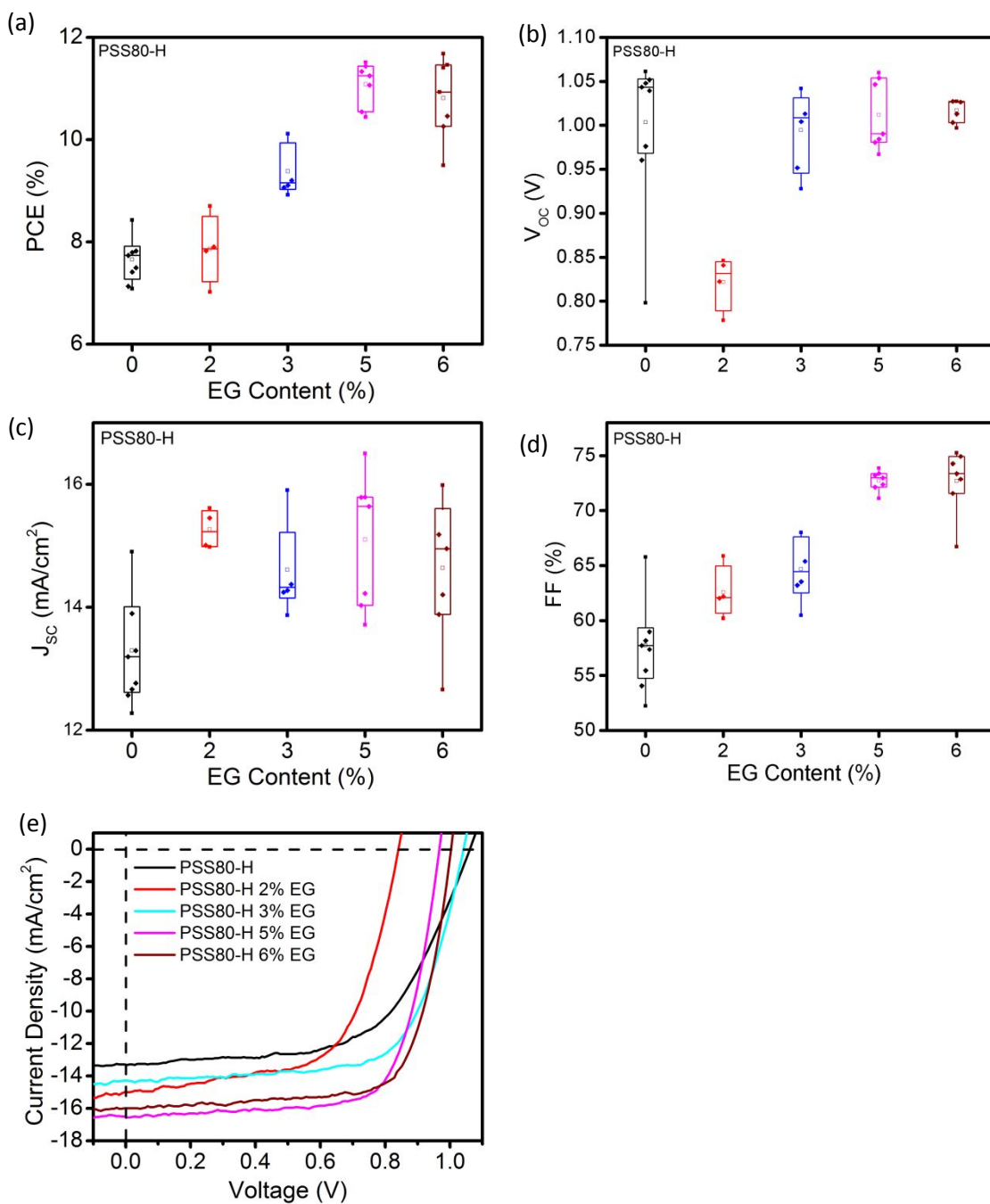


Figure S10. Statistics of (a) PCE, (b) V_{oc} , (c) J_{sc} , and (d) FF of the MAPbI₃ PVSCs based on PSS80-H with and without EG. (e) J - V curves of the best performance MAPbI₃ PVSCs based on pristine and 2, 3, 5 and 6 vol% EG treated PSS80-H HTLs.

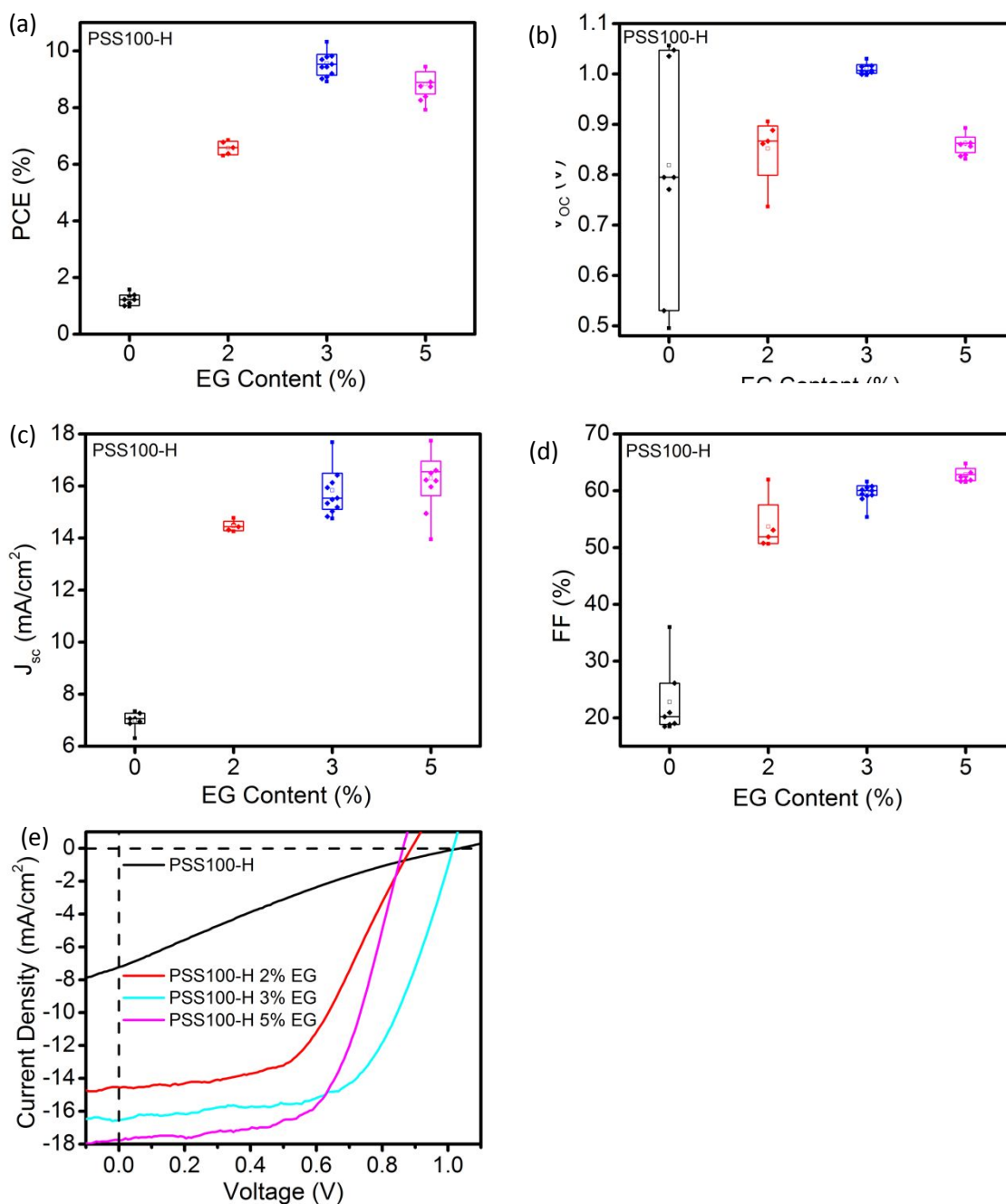


Figure S11. Statistics of (a) PCE, (b) V_{oc} , (c) J_{sc} , and (d) FF of the MAPbI₃ PVSCs based on PSS100-H with and without EG. (e) $J-V$ curves of the best performance MAPbI₃ PVSCs based on pristine and 2, 3, and 5 vol% EG treated PSS100-H HTLs.

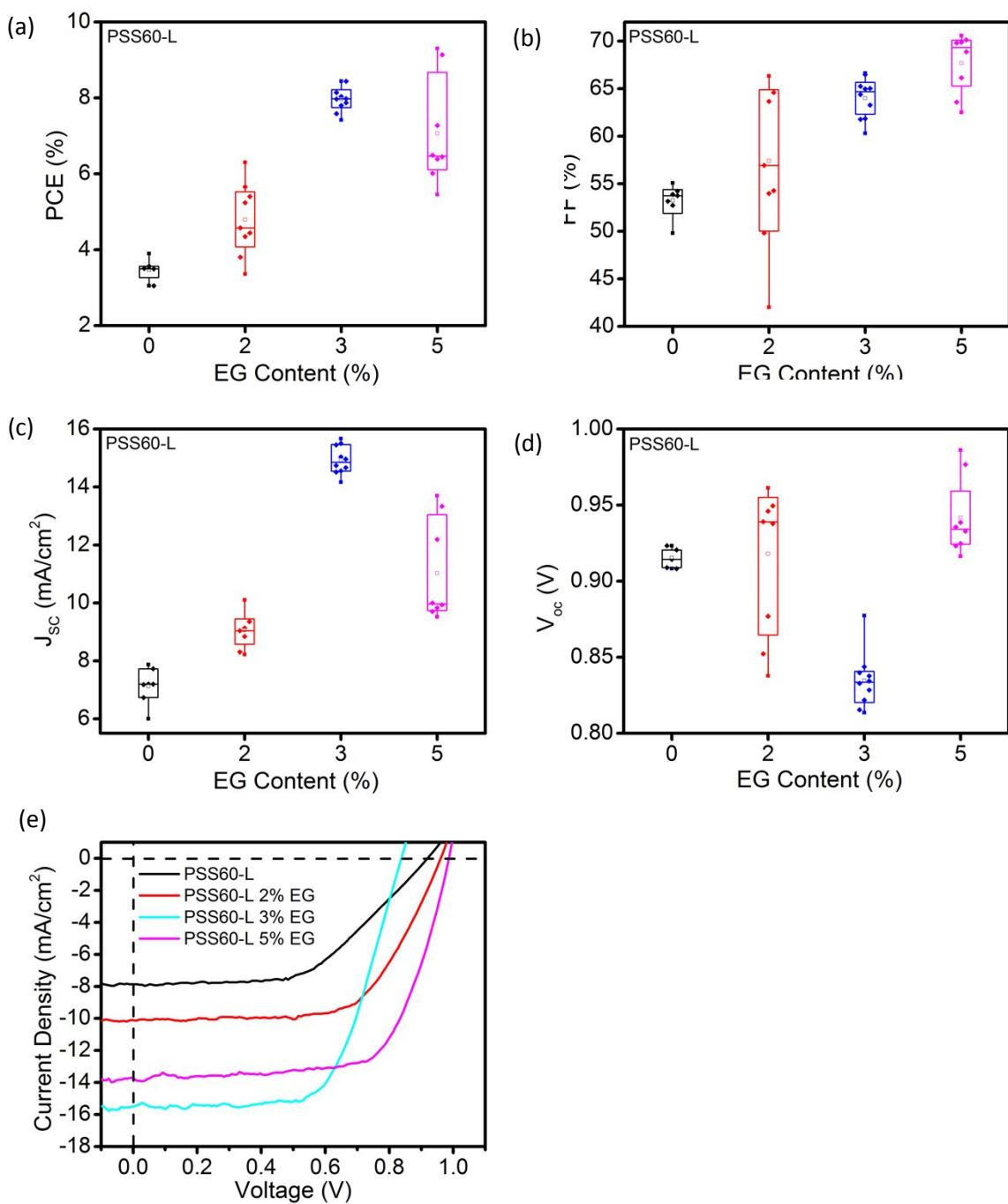


Figure S12. Statistics of (a) PCE, (b) V_{oc} , (c) J_{sc} , and (d) FF of the MAPbI₃ PVSCs based on PSS60-L with and without EG. (e) J - V curves of the best performance MAPbI₃ PVSCs based on pristine and 2, 3, and 5 vol% EG treated PSS60-L HTLs.

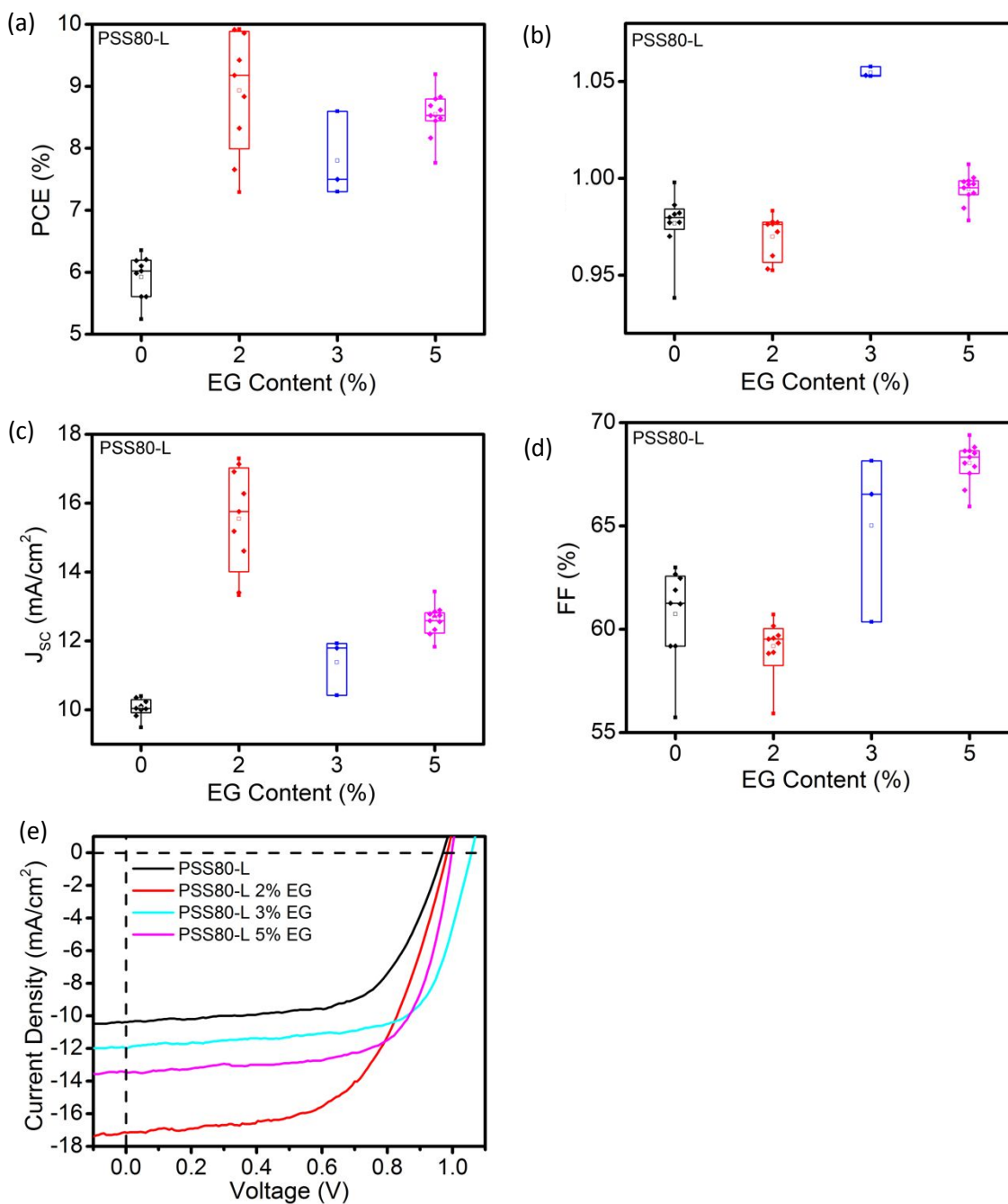


Figure S13. Statistics of (a) PCE, (b) V_{oc} , (c) J_{sc} , and (d) FF of the MAPbI₃ PVSCs based on PSS80-L with and without EG. (e) $J-V$ curves of the best performance MAPbI₃ PVSCs based on pristine and 2, 3, and 5 vol% EG treated PSS80-L HTLs.

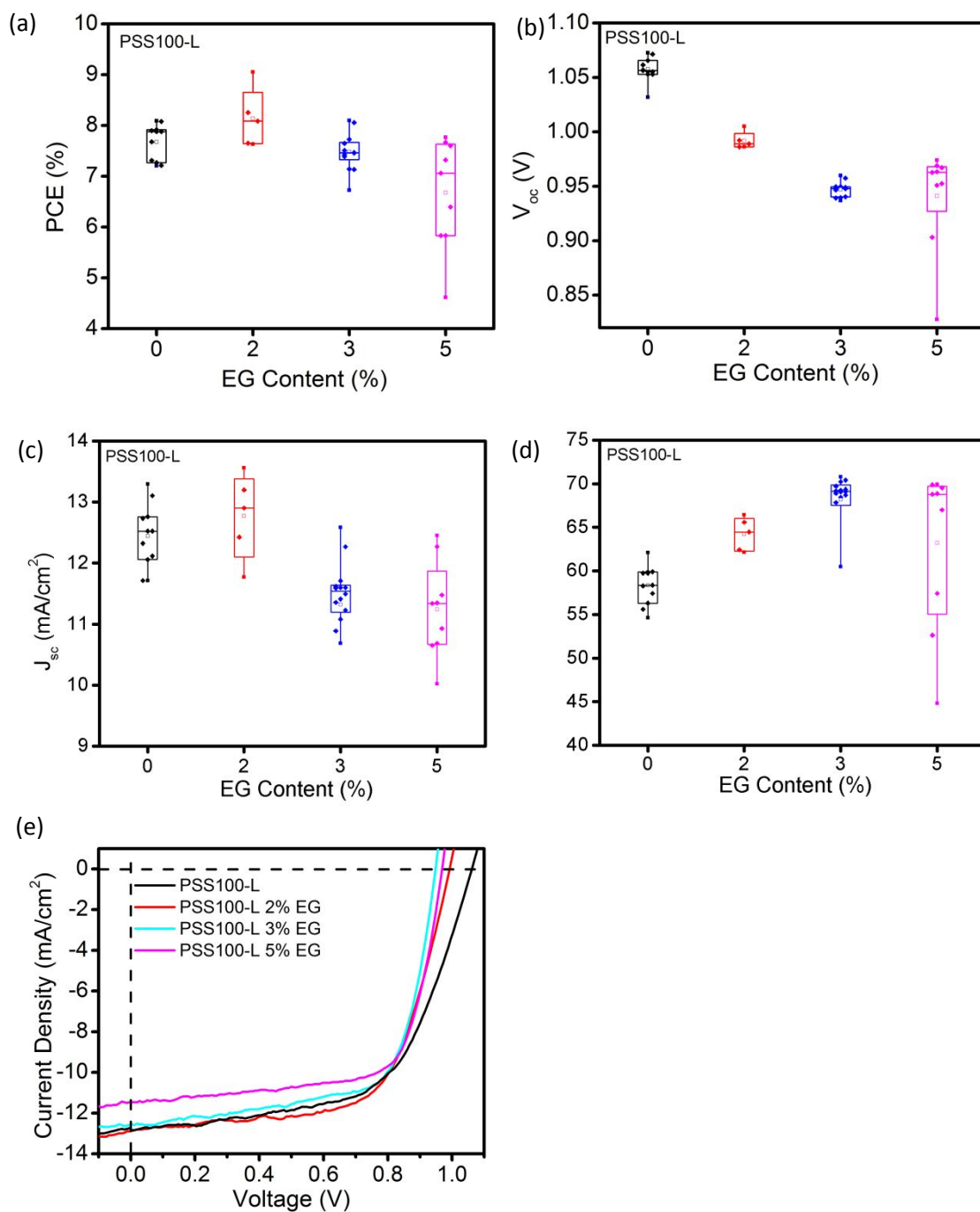


Figure S14. Statistics of (a) PCE, (b) V_{oc} , (c) J_{sc} , and (d) FF of the MAPbI₃ PVSCs based on PSS100-L with and without EG. (e) $J-V$ curves of the best performance MAPbI₃ PVSCs based on pristine and 2, 3, and 5 vol% EG treated PSS100-L HTLs.

Reference

- (1) Elschner, A.; Kirchmeyer, S.; Lovenich, W.; Merker, U.; Reuter, K. *PEDOT: Principles and Applications of an Intrinsically Conductive Polymer*; CRC Press: 2010.
- (2) Lee, T. W.; Chung, Y. S. Control of the Surface Composition of a Conducting-polymer Complex Film to Tune the Work Function. *Adv. Funct. Mater.* **2008**, *18*, 2246-2252.
- (3) Horii, T.; Hikawa, H.; Katsunuma, M.; Okuzaki, H. Synthesis of Highly Conductive PEDOT:PSS and Correlation with Hierarchical Structure. *Polymer* **2018**, *140*, 33-38.
- (4) Kazuhiro, A.; Tatsuji, A. Method of Producing Conductive Polymer Particle Dispersion, and Method of Producing Electrolytic Capacitor Using Conductive Polymer Particle Dispersion. U.S. Patent 9,892,859, Feb. 12, 2018.
- (5) Ha, Y. H.; Nikolov, N.; Pollack, S. K.; Mastrangelo, J.; Martin, B. D.; Shashidhar, R. Towards a Transparent, Highly Conductive Poly(3,4-ethylenedioxythiophene). *Adv. Funct. Mater.* **2004**, *14*, 615-622.
- (6) Zheng, E.; Jain, P.; Dong, H.; Niu, Z.; Chen, S.; Zhong, S.; Yu, Q. Chemical Polymerization of Hydroxymethyl and Chloromethyl Functionalized PEDOT:PSS. *ACS Appl. Polym. Mater.* **2019**, *1*, 3103–3114.
- (7) Richardson, B. J.; Zhu, L.; Yu, Q. Inverted Hybrid Solar Cells Based on Pyrite FeS₂ Nanocrystals in P3HT:PCBM with Enhanced Photocurrent and Air-stability. *Sol. Energy Mater. Sol. Cells* **2013**, *116*, 252-261.